International Journal of Engineering Research and Science & Technology

A Two-Stage AC–DC Converter with ANFIS Control for Simultaneous Dual-Battery Charging in Electric Vehicle

Mr. P.Abdul Raheem Khan[1], G.Chandrika[2], A.Akhileswar[3], G.Sivanjaneyulu[4], S.Mahammad Ghouse[5]

[1]Assistant Professor, Department of EEE, AITS, Kadapa

[2,3,4,5] Student (UG), Department of EEE, AITS, Kadapa

Abstract—

For use in electric vehicle (EV) applications, this study details a two-stage AC-DC power conversion architecture that can charge two batteries at once. Starting with a three-phase multilevel boost PFC converter and continuing with an isolated bidirectional dual-output DC-DC converter capable of zero-voltage switching (ZVS), this is the topology that has been suggested. The AC-DC stage can work in continuous conduction mode (CCM) unaffected by duty-cycle fluctuations in the DC-DC stage since the two stages run separately. The DC-link voltage is regulated and the two battery outputs are made to share power equally using an Adaptive Neuro-Fuzzy Inference System (ANFIS)–based control technique, which improves the system's performance. With the ANFIS controller, you may enhance dynamic responsiveness, decrease total harmonic distortion (THD), and achieve a power factor close to unity regardless of the load or battery status. The suggested dual-battery charger is analyzed in detail, including its operational principle. Extensive Matlab/Simulink results were produced to validate the efficacy and practicality of the proposed system.

I. INTRODUCTION

The importance of electric mobility in enhancing transportation sustainability and efficiency is growing. The main reasons for the shift from ICE to EVs are the goals of reducing pollution and noise pollution and the need to create a cleaner, safer environment [1, 2]. In addition, research has shown that compared to ICE cars, EVs are far more efficient and cost-effective to operate [3]. As a result, businesses and academics all around the globe are pushing for more EV use to help the environment. Even while electric vehicles are great for the environment, the power that powers them is typically derived from finite fossil fuels, which in turn release greenhouse gases. One more sustainable way to charge electric vehicles is to include non-traditional energy sources into the grid [4]-[6]. To further reduce power quality concerns while charging EV batteries linked to the grid, sophisticated control tactics are required. There are two main types of electric vehicle chargers: on-board, which are more convenient but slower, and off-board, which offer faster charging but require more infrastructure. The two primary roles of an electric vehicle charger are controlling the charging voltage of the battery and regulating the DC-link voltage to maintain power quality [7]. Electric vehicle chargers can be designed as either one-stage AC-DC converters or two-stage AC-DC + DC-DC converters, as stated in the literature. To control the voltage of the batteries and enhance the quality of the grid power, single-stage AC-DC converters combine line-frequency rectifiers with isolated or

non-isolated DC-DC converters [8]. When operating under dynamic load situations, however, these converters need sophisticated control algorithms to regulate both the DC-link voltage and the charging of the batteries at the same time. The flexibility, increased efficiency, and less component stress of two-stage AC-DC converters make them the preferable choice for high-power applications [9]. These converters consist of an active power factor correction (PFC) stage and an isolated DC-DC stage [10]. For high-voltage, high-power applications, three-phase active PFC converters have certain advantages over their single-phase equivalents. The current body of research on two-stage electric vehicle chargers draws attention to a number of disadvantages, such as larger size, more control complexity, switching losses, and an increase in component count [11]-[16]. When it comes to charging high-voltage and low-voltage batteries, for example, there have been proposals for dual-output DC-DC converters. However, problems including circulating currents, complicated management techniques, and poor power quality still remain. A two-stage three-phase AC-DC converter with a dual-output isolated DC-DC stage is proposed in this study to overcome these issues [17] – [20]. It can charge two electric vehicle batteries with the same or different voltage ratings at the same time. The suggested solution relies on a controller that balances the power distribution between the two battery outputs and controls the DC-link voltage using an Adaptive Neuro-Fuzzy Inference solution (ANFIS). By integrating neural networks' learning capabilities with fuzzy logic's rule-based reasoning, the ANFIS controller achieves near-unity power factor under variable load and battery circumstances, reduces total harmonic distortion (THD), and improves dynamic responsiveness [21] – [27]. A modular three-phase AC-DC converter and a dual-output bidirectional DC-DC converter with zero-voltage switching (ZVS) are used in the proposed charger to reduce switching losses and maximize efficiency. The converters allow for a broad variety of input and output voltages. The suggested topology is shown successful using Matlab/Simulink simulations in regards to power quality, dynamic responsiveness, and dual-battery charging performance.

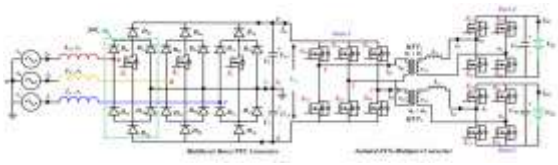


Fig. 1. Block Diagram of the Proposed system

II. EV CHARGER CONFIGURATION AND CONTROL STRATEGY

A. Dual-Battery Charger Configuration

The proposed EV charger consists of a three-phase multilevel boost PFC (MBPFC) converter as the front-end, cascaded with an isolated zero-voltage switching multiport DC–DC converter (ZVS-MPC) for simultaneous charging of two EV batteries, as shown in Fig. 1. In the MBPFC stage, each phase $j \in \{a, b, c\}$is equipped with a source-side inductor $L_j$and internal resistance r_j. Each phase includes a bipolar bidirectional switch SW_jconnected to upper and lower groups of fast-recovery diodes $D_{jp}$and D_{jq}, forming a multilevel topology. The DC-link voltage is obtained across two midpoint capacitors $C_1$and C_2, providing a balanced DC voltage output. The single bipolar bidirectional switch for phase a, SW_a, is implemented using a controlled

switch $S_a$integrated with a diode bridge $D_{a1} - D_{a4}$and connected to the mid-point $N$to maintain capacitor voltage balance. The MBPFC stage interfaces with the ZVS-MPC, which includes a three-leg full-bridge converter on the primary side (port 1) and two two-leg full-bridge converters on the secondary side (ports 2 and 3) to provide two isolated DC outputs. Each secondary output is connected to a high-frequency transformer (HFT_1 and HFT_2) with turns ratios $n_1 : n_2$and $n_3 : n_4$, providing galvanic isolation. The absence of direct leakage inductance across the secondary ports minimizes circulating currents between outputs. The ZVS operation across all switches reduces switching losses and improves system efficiency, while enabling bidirectional operation for energy recovery and controlled power sharing between the two battery outputs.

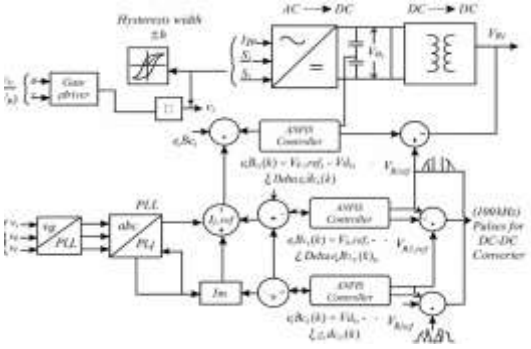


Fig. 2. Proposed controller block diagram

B. Control Strategy

The control strategy targets the following objectives:

1. Unity power factor (UPF) operation with sinusoidal source currents.

2. DC-link voltage regulation to stabilize the MBPFC output.

3. Simultaneous and balanced charging of two EV batteries via the ZVS-MPC.

1) MBPFC Control

The MBPFC employs hysteresis current control to track a sinusoidal reference current $i_{j,ref}$derived from the DC-link voltage controller:

$$i_{j,ref} = I_{m,ref} \frac{v_j}{V_m}$$

where $I_{m,ref}$and $V_m$are the peak amplitudes of the source current and voltage, respectively. A phase-locked loop (PLL) synchronizes the source current with the AC voltage. Hysteresis control generates switching pulses $S_j$for the MBPFC switches S_a, S_b, S_cas follows:

$$S_j = \begin{cases} 1, & i_j < i_{j,ref} - h \\ 0, & i_j > i_{j,ref} + h \end{cases}$$

where $\Delta i_j = i_{j,ref} - i_j$and $h$is the hysteresis band width. A zero-sequence current $i_0$is added to maintain voltage balance across the DC-link capacitors:

$$i_{j,ref} = i_{j,ref} + i_0$$

2) ZVS-MPC Control with ANFIS

The dual-output ZVS-MPC regulates the battery voltages $V_{B1}$and V_{B2}through phase-shift control, with phase shifts $d_1$and $d_2$corresponding to ports 2 and 3. To achieve simultaneous and independent battery charging, a PI controller generates reference phase shifts based on the voltage errors at each battery terminal.

To enhance dynamic performance and ensure balanced power distribution, the PI controller is replaced by an ANFIS-based controller. The ANFIS controller integrates the learning capability of neural networks with fuzzy logic reasoning to:

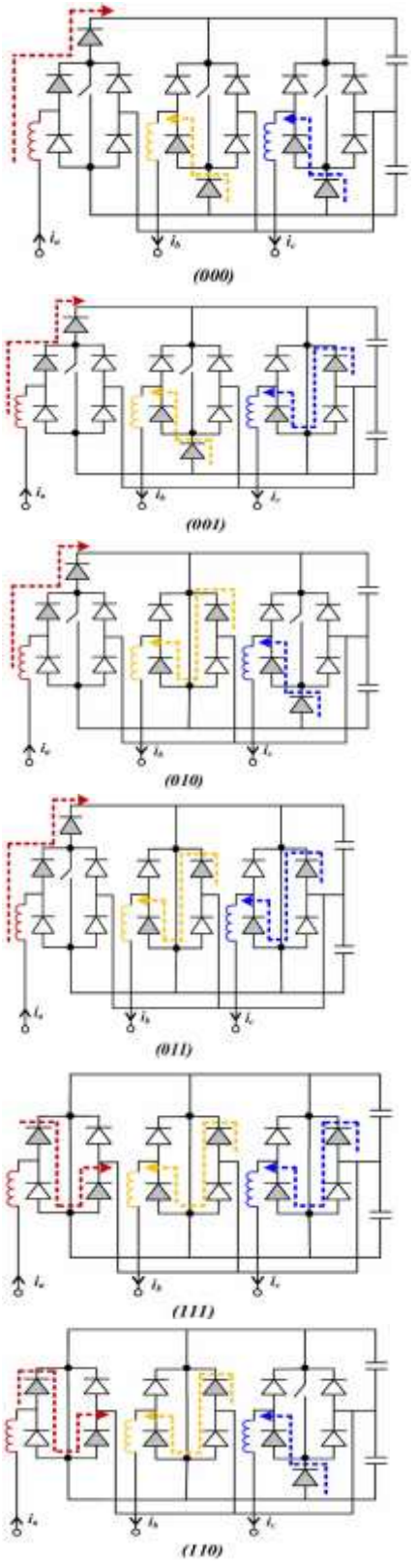
- Adjust the phase shifts $d_1$and $d_2$in real-time.
- Compensate for battery state-of-charge (SOC) variations and unequal loading.
- Minimize transient voltage deviations and ensure proportional current sharing.

This strategy enables efficient dual-battery charging, reduces total harmonic distortion (THD), and maintains near-unity power factor under varying input voltage and load conditions.

III. OPERATING ANALYSIS OF THE PROPOSED BATTERY CHARGER

The operating principle of the proposed three-phase MBPFC converter relies on the bipolar bidirectional switches $SW_j (j \in \{a, b, c\})$ and the direction of the input source currents i_j. In continuous conduction mode (CCM), the phase-a pole voltage $v_{a0}$is determined by the ON/OFF states of the controlled switch $S_a$and the polarity of i_a. During the positive half-cycle of the input current ($i_a > 0$), the inductor current charges when $S_a$is ON, producing zero pole voltage, and discharges through $V_{dc}/2$when $S_a$is OFF. Conversely, during the negative half-cycle ($i_a < 0$), the pole voltage alternates between zero and $-V_{dc}/2$depending on the switch state. Each bipolar bidirectional switch effectively operates as a single-phase PFC converter, producing a DC-link voltage $V_{dc} = 2V_m \mid \sin \omega t \mid /(1 - \delta(t))$, where $\delta(t)$is the PFC duty cycle. This charging and discharging cycle repeats every AC period, resulting in sinusoidal source currents. The three-phase MBPFC divides the input AC waveform into six 60° sectors based on voltage polarity. Within each sector, the switching states $S_j$determine the pole voltages and DC-link capacitor currents, while the midpoint current $i_N$may create a voltage imbalance between $C_1$and C_2. A zero-sequence current $i_0$is therefore added to the reference current to maintain $V_{C1} = V_{C2} = V_{dc}/2$and ensure balanced capacitor voltages. The isolated ZVS-multiport DC–DC converter is composed of six primary switches ($S_{11} - S_{16}$) and eight secondary switches ($S_{21} - S_{24}$ for port 2, $S_{31} - S_{34}$for port 3). For grid-to-vehicle (G2V) operation, two identical high-frequency transformers (HFTs) with turns ratios of 1:1 provide isolated outputs $V_{B1}$and V_{B2}. The phase-shift ratios $d_1$and $d_2$control power flow to ports 2 and 3, respectively, while the primary switch duty cycles remain fixed. The converter operates over four intervals in each switching cycle. In the first interval, the primary voltage transitions from negative to positive while current naturally flows through the antiparallel diodes of inactive switches, enabling zero-voltage switching (ZVS) as the corresponding switches turn ON when current reaches zero. In the second interval, the secondary voltages change polarity and the leakage inductances control current ramping to the batteries. In the third interval, primary switches are turned OFF, the secondary voltages reverse, and currents flow through diodes, again achieving ZVS for complementary switches. Finally, in the fourth interval, complementary secondary switches are turned ON, maintaining proper current directions and ensuring continuous bidirectional power transfer. Throughout all intervals, the ZVS operation minimizes switching losses, while the ANFIS-based controller dynamically adjusts phase shifts $d_1$and $d_2$to regulate battery voltages and ensure balanced charging currents according to the state of charge and load conditions. This integrated MBPFC and ZVS-MPC operation enables efficient dual-battery charging, high efficiency, reduced harmonic distortion, and near-unity power factor under varying input and load conditions. The proposed architecture

ensures precise power sharing, maintains DC-link voltage stability, and supports independent and simultaneous charging of two EV batteries.



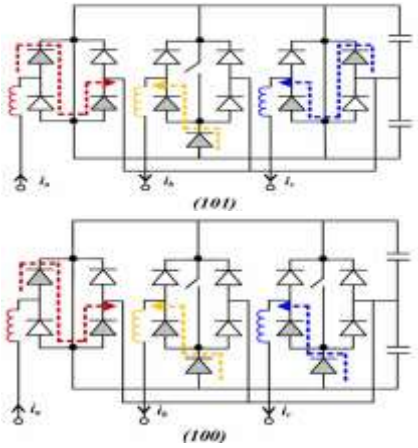


Fig. 3. PFC converter equivalent circuits $(v_a > 0, v_b < 0, v_c < 0)$ illustrating the dependence of the capacitive midpoint current i_N on the switching state S_j for $\theta \in \left(-\frac{\pi}{3}, \frac{\pi}{3}\right)$.

Mode 1 ($t_0 < t < t_1$)

During this interval, switches S_{12}, S_{13}, and S_{16} are OFF, and the primary voltages (v_{p1}, v_{p2}) transition from negative to positive. The currents (i_{p1}, i_{p2}) naturally commutate from switches S_{12}, S_{13}, and S_{16} to antiparallel diodes D_{11}, D_{14}, and D_{15}, respectively. Switches S_{11}, S_{14}, and S_{15} turn ON under zero-voltage switching (ZVS) conditions once the secondary currents reach zero at instants Z_1 and Z_2.

The secondary winding currents during this interval are given by

$$i_{s1}(t) = i_{s2}(t) = \frac{N_1 V_{dc} + V_{B1}}{L_1}(t - t_0) + i_{s1}(t_0),$$

where N_1 is the transformer turns ratio and $L_1 = L_2$.

Mode 2 ($t_1 < t < t_2$)

At t_1, switches S_{22}, S_{23}, S_{32}, and S_{33} are turned OFF, causing the secondary voltages (v_{s1}, v_{s2}) to change polarity. The voltages across leakage inductors L_1 and L_2 become $(N_1 V_{dc} - V_{B1})$ and $(N_1 V_{dc} - V_{B2})$, respectively. The secondary current expressions are

$$i_{s1}(t) = i_{s2}(t) = \frac{N_1 V_{dc} - V_{B1}}{L_1}(t - t_1) + i_{s1}(t_1).$$

Mode 3 ($t_2 < t < t_3$)

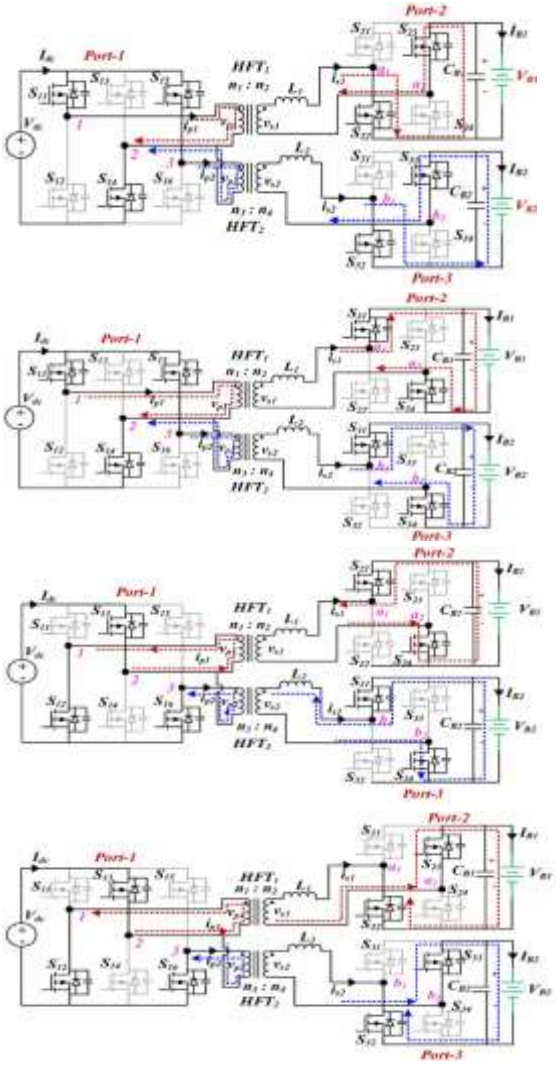
During this interval, switches S_{11}, S_{14}, and $S_{15}$are turned OFF, and the secondary voltages reverse polarity. The current commutates to diodes D_{12}, D_{13}, and D_{16}, enabling ZVS turn-ON of switches S_{12}, S_{13}, and S_{16}. The secondary currents are expressed as

$$i_{s1}(t) = i_{s2}(t) = \frac{-N_1 V_{dc} + V_{B1}}{L_1}(t - t_2) + i_{s1}(t_2).$$

Mode 4 ($t_3 < t < t_4$)

At t_3, switches S_{21}, S_{24}, S_{31}, and $S_{34}$are turned OFF, while switches S_{22}, S_{23}, S_{32}, and $S_{33}$are turned ON. The secondary voltages reverse polarity again, and the secondary winding currents are given by

$$i_{s1}(t) = i_{s2}(t) = \frac{-N_1 V_{dc} + V_{B1}}{L_1}(t - t_3) + i_{s1}(t_3).$$



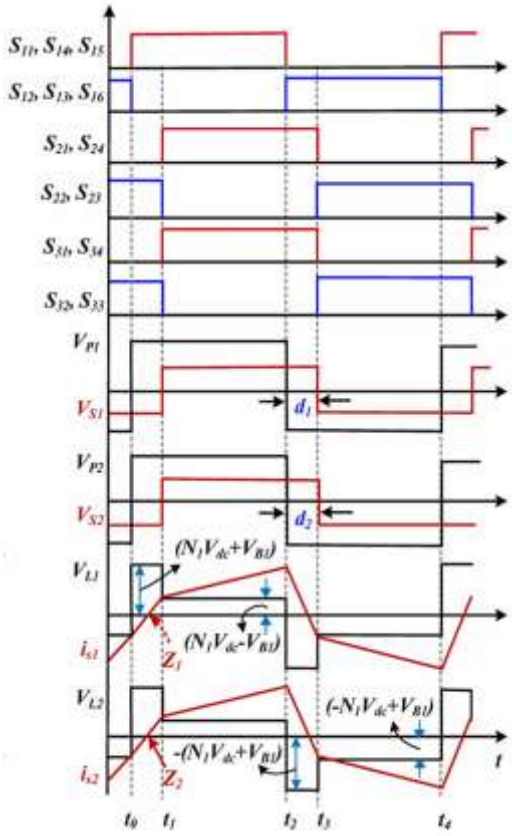


Fig. 4. Switching intervals and operating modes of isolated ZVS multiport converter (ZVS-MPC): (a)–(d) four operating intervals within one switching period; and (e) associated analytical waveforms.

IV. RESULTS AND DISCUSSION

The proposed dual-battery EV charger configuration was simulated in MATLAB/Simulink to validate the theoretical analysis. The simulation parameters are summarized, while hardware component specifications used for experimental validation are listed. A laboratory prototype was developed for a reduced source voltage, and the experimental setup is shown in Figure. Simulation and experimental results are presented side-by-side to facilitate performance verification. Figure illustrate the three-phase input voltages (v_a, v_b, v_c) of 220 V and source currents (i_a, i_b, i_c) of 20 A. Figure shows the source current $i_a$in

phase with the corresponding source voltage v_a, confirming that the proposed charger achieves near-unity power factor. The DC-link voltage is maintained at 400 V, with a corresponding current of 12.8 A, as shown in Figure. These results demonstrate close agreement between experimental and simulation waveforms.

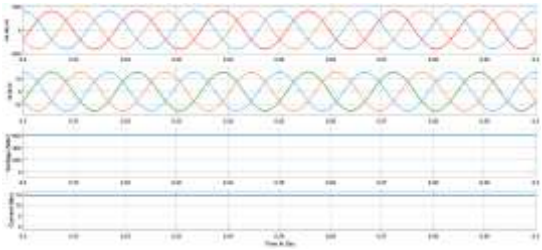


Fig. 5. Simulated and test results of PFC converter (a) phase voltages (va,vb,vc) (b) phase currents (ia,ib,ic) (c) Rectified voltage (Vdc) and current (Idc).

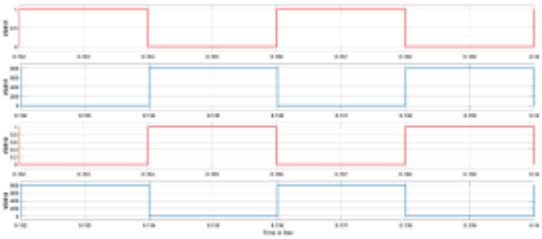


Fig. 6. Simulated and test results of ZVS-MPC (a) & (b) Port1 ZVS operation of switch S11 & S12.

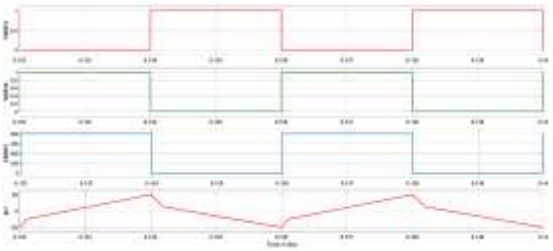


Fig. 7. Simulated and test results of switching pulses for S13, S14 and switch voltage VDS13, current ip1.

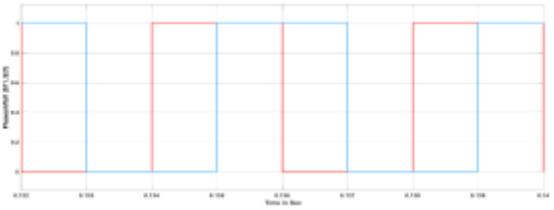


Fig. 8. Simulation and test results of Phase shift d1 between port1 and port2.

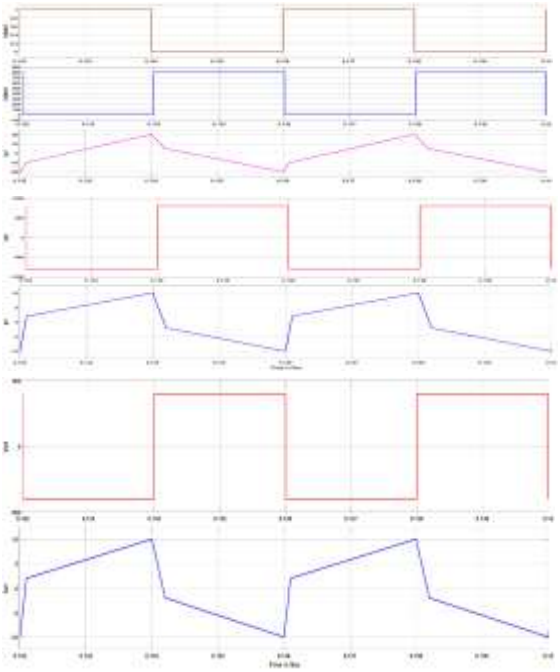


Fig. 9. Simulated and test results of DC-DC converter (a) primary side voltage/current of HFT1, (b) secondary side voltage/current of HFT1.

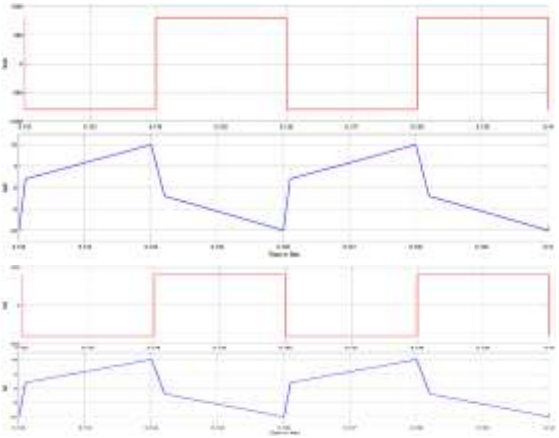


Fig. 10. Simulation and test results of ZVS-MPC (a) voltage/current of secondary winding of HFT2,(b)

voltage/current of secondary winding HFT2.

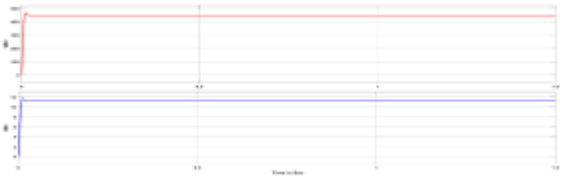


Fig. 11. Simulation and test results of ZVS-MPC (a) port 2 output volt age/current, (b) Port 3 output voltage /current

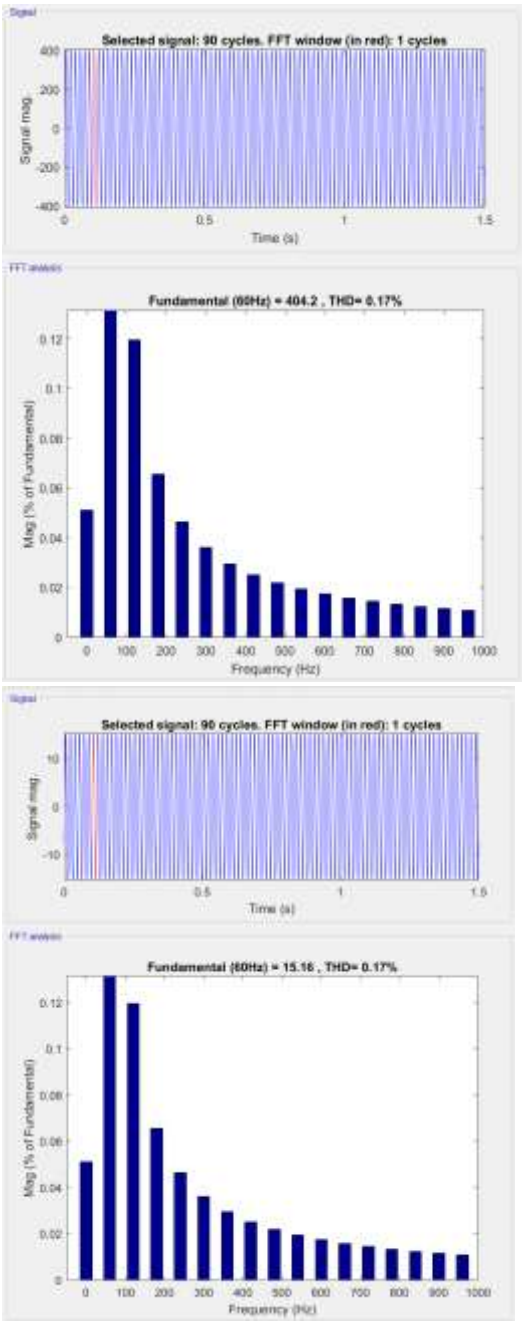


Fig. 12 presents the total harmonic distortion (THD) of the source voltage and source current.

The THD remains well within the limits specified by IEEE-519, confirming effective harmonic mitigation by the proposed control strategy. The power factor is maintained very close to unity over the entire operating range, demonstrating robust PFC operation under varying load conditions. The ZVS operation of the multiport DC–DC converter (MPC) is verified in Figures. Gating signals and corresponding switch voltages ($V_{DS11}, V_{DS12}, V_{DS13}, V_{DS14}$) along with primary currents (i_{p1}) demonstrate that the switches turn on under zero-voltage conditions, reducing switching losses and enhancing overall efficiency. The phase-shift control between the primary and secondary sides, as illustrated in Figure, enables proper power flow and simultaneous charging of the two battery outputs. Figures show primary and secondary voltages and currents of HFT1 and HFT2, confirming that both secondary ports deliver equal power. Figure illustrates the output voltages and currents at ports 2 and 3, with $V_{B1} = V_{B2} = 190\text{V}$ and $I_{B1} = I_{B2} = 8\text{A}$, validating balanced power distribution. Further experimental observations demonstrate stable operation of the MBPFC and MPC stages under a supply voltage of 220 V, supply current of 10 A, primary-side voltage of 200 V, and primary leakage inductance current of 8 A. The MPC switching frequency of 100 kHz was verified, and the zoomed waveforms confirm ZVS operation with zero turn-on losses. Overall, the results indicate that the proposed two-stage dual-battery charger operates smoothly and efficiently,

maintains high power quality in terms of THD and power factor, provides a wide input and output voltage range, and ensures balanced power sharing between the two battery ports. The measured efficiency of the system under rated load conditions is 94.83%, highlighting the effectiveness of the proposed topology for practical EV charging applications.

V. CONCLUSION

This paper presented a two-stage AC–DC EV charger capable of simultaneously charging two batteries with equal or different voltage ratings. The proposed configuration integrates a three-phase multilevel boost PFC converter with an isolated ZVS-multiport DC–DC converter, enabling high-efficiency bidirectional power flow and precise power sharing between the two battery ports. An ANFIS-based controller was implemented to regulate the DC-link voltage and ensure balanced charging, enhancing dynamic performance, reducing THD, and achieving near-unity power factor under varying input and battery conditions. Simulation and experimental results demonstrated that the proposed charger delivers sinusoidal, in-phase source currents, maintains balanced DC-link voltages, achieves ZVS operation across all switches, and provides efficient dual-battery charging. The charger attained an efficiency of 94.83% under rated load conditions, confirming its suitability for high-power EV applications. Overall, the proposed topology offers a reliable, high-performance solution for off-board dual-battery EV charging, combining modularity, power quality improvement, and robust control for practical implementation.

REFERENCES

[1] A. Emadi, Y. J. Lee, and K. Rajashekara, “Power electronics and motor drives in electric, hybrid electric, and plug-in hybrid electric vehicles,” *IEEE Trans. Ind. Electron.*, vol. 55, no. 6, pp. 2237–2245, Jun. 2008.

[2] M. Ehsani, Y. Gao, S. E. Gay, and A. Emadi, *Modern Electric, Hybrid Electric, and Fuel Cell Vehicles: Fundamentals, Theory, and Design*, 2nd ed. CRC Press, 2009.

[3] C. C. Chan, “The state of the art of electric, hybrid, and fuel cell vehicles,” *Proc. IEEE*, vol. 95, no. 4, pp. 704–718, Apr. 2007.

[4] “A New Configuration of Nine Level Switched Capacitor Boost Inverter of Single DC Source with Reduced Component Count”, *Int Res J Adv Engg Hub*, vol. 3, no. 10, pp. 3919–3924, Oct. 2025.

[5] R. Erickson and D. Maksimovic, *Fundamentals of Power Electronics*, 2nd ed. Springer, 2001.

[6] L. M. Tolbert, F. Z. Peng, and T. G. Habetler, “Multilevel converters for large electric drives,” *IEEE Trans. Ind. Appl.*, vol. 35, no. 1, pp. 36–44, Jan./Feb. 1999.

[7] P. C. Loh, D. G. Holmes, and T. A. Lipo, “Carrier-based PWM methods for multilevel converters,” *IEEE Trans. Ind. Electron.*, vol. 49, no. 4, pp. 858–867, Aug. 2002.

[8] Balaji, A. ., & Reddy, K. M. . (2023). An Interlinking Converter for Renewable Energy Integration into Hybrid Grids. *Journal of Energy Engineering and Thermodynamics*, *3*(02), 12–21.

[9] J. Rodriguez, J. S. Lai, and F. Z. Peng, “Multilevel inverters: A survey of topologies, controls, and applications,” *IEEE Trans. Ind. Electron.*, vol. 49, no. 4, pp. 724–738, Aug. 2002.

[10] H. Abu-Rub, J. Holtz, J. Rodriguez, and G. Baoming, "Medium-voltage multilevel converters—State of the art, challenges, and requirements in industrial applications," *IEEE Trans. Ind. Electron.*, vol. 57, no. 8, pp. 2581–2596, Aug. 2010.

[11] R. Roopa Sri, & K. Meenendranath Reddy. (2023). Improved Power Management Control of a Multiport Converter Based EV Charging Station with PV and Battery. *International Journal of Research in Science & Engineering* , *3*(02), 16–25.

[12] B. Singh, S. S. Murthy, and S. Gupta, "High-performance PWM AC–DC converters," *IEEE Trans. Ind. Electron.*, vol. 46, no. 3, pp. 525–536, Jun. 1999.

[13] F. Z. Peng, J. S. Lai, and L. M. Tolbert, "Multilevel converters for electric vehicle applications," in *Proc. IEEE Vehicle Power and Propulsion Conf.*, 2003, pp. 349–354.

[14] S. Jain and V. Agarwal, "A single-phase grid-connected inverter for PV systems with ripple current reduction," *IEEE Trans. Power Electron.*, vol. 22, no. 5, pp. 1920–1930, Sep. 2007.

[15] Balapanoori Sai Sudheer, K. Meenendranath Reddy, "Realizing A Single-Stage Hybrid Pv System Using Fuzzy with Battery Current-Sharing Power Decoupling Method", In Journal of Engineering Sciences, Vol 14 Issue 08, Aug 2023.

[16] Sushma Babburi. (2025). Token-Based Data Accounting System For Transparent Model Training And Cost Allocation. American Journal of AI Cyber Computing Management, 5(4), 463–474. https://doi.org/10.64751/ajaccm.2025.v5.n4.pp463-474.

[17] J. Rodriguez, S. Bernet, B. Wu, J. O. Pontt, and S. Kouro, "Multilevel voltage-source-converter topologies for industrial medium-voltage drives," *IEEE Trans. Ind. Electron.*, vol. 54, no. 6, pp. 2930–2945, Dec. 2007.

[18] F. Z. Peng, J. S. Lai, and L. M. Tolbert, "Multilevel converters for electric vehicle applications," in *Proc. IEEE Vehicle Power and Propulsion Conf.*, 2003, pp. 349–354.

[19] B. Singh, S. S. Murthy, and S. Gupta, "Analysis of a three-phase PWM AC–DC converter," *IEEE Trans. Power Electron.*, vol. 13, no. 4, pp. 725–731, Jul. 1998.

[20] Ganji, M. (2025). Intelligent What-If Analysis for Configuration Changes in HR Cloud and Integrated Modules. International Journal of All Research Education and Scientific Methods, 13(04), 4828–4835. https://doi.org/10.56025/ijaresm.2025.1304254828.

[21] Cyril, H. P. (2025). Event-Driven Provisioning Architectures For Modern Telecom Networks: Overcoming Legacy Limitations And Enabling Autonomous 6g Operations. International Journal of Advanced Research in Computer Science, 16(6), 75–82. https://doi.org/10.26483/ijarcs.v16i6.7389.

[22] Todupunuri, A. (2024). Develop Machine Learning Models to Predict Customer Lifetime Value for Banking Customers, Helping Banks Optimize Services. International Journal of All Research Education & Scientific Methods, 12(10), 1254–1259. https://doi.org/10.56025/ijaresm.2024.1210241254.

[23] J. Rodriguez, J. Lai, and F. Z. Peng, "Multilevel inverters: A survey of topologies, controls, and applications," *IEEE Trans. Ind. Electron.*, vol. 49, no. 4, pp. 724–738, Aug. 2002.

[24] L. M. Tolbert and F. Z. Peng, "Multilevel converters for large electric

drives," *IEEE Trans. Ind. Appl.*, vol. 35, no. 1, pp. 36–44, Jan./Feb. 1999.

[25] S. Kouro, M. Malinowski, K. Gopakumar, J. Pou, L. G. Franquelo, B. Wu, J. Rodriguez, and M. A. Perez, "Recent advances and industrial applications of multilevel converters," *IEEE Trans. Ind. Electron.*, vol. 57, no. 8, pp. 2553–2580, Aug. 2010.

[26] Kalyan, R. ., Subbaiah, M. V. ., Charan, B. S. ., Reddy, K. M. ., & Babu, D. P. S. . (2022). Modelling and Control of SEPIC and BIDC Converter Based off-Board EV Battery Charger using PV Array. *Journal of Energy Engineering and Thermodynamics*, *2*(04), 36–45.

[27] J. Holtz, H. Abu-Rub, and J. Rodriguez, "Control of multilevel voltage source inverters," *Proc. IEEE*, vol. 105, no. 11, pp. 2101–2116, Nov. 2017.